Desalination and Water Treatment
www.deswater.com
doi: 10.5004/dwt.2021.26608

211 (2021) 45–59
January

Sensitivity analysis of *N* alike partly covered PVT flat plate collectors integrated double slope solar distiller unit

Kiran Bharti[a], Shalini Manwal[b], Chandra Kishore[b], Rakesh Kumar Yadav[c], Prabhakar Tiwari[d], Desh Bandhu Singh[b,*]

[a]*Saraswati Institute of Engineering and Technology, 24KM Stone, NH-24, Pilakhuwa, Ghaziabad, Uttar Pradesh, India, email: kiran166bharti@gmail.com*
[b]*Department of Mechanical Engineering, Graphic Era (Deemed to be University), Bell Road, Clement Town, Dehradun, Uttarakhand – 248001, India, emails: Deshbandhusingh.me@geu.ac.in (D. Bandhu Singh), manwalshalini@gmail.com (S. Manwal), chandrakishore@geu.ac.in (C. Kishore)*
[c]*KCC Institute of Technology and Management, Greater Noida – 201306, Uttar Pradesh, India, email: er.rakeshyadava@gmail.com*
[d]*Madan Mohan Malviya University of Technology, Gorakhpur – 273008, Uttar Pradesh, India, email: profptiwari@gmail.com*

Received 1 April 2020; Accepted 19 September 2020

ABSTRACT

In this research paper, the sensitivity analysis of *N* alike in parts covered photovoltaic thermal flat plate collectors integrated double slope solar distiller unit is performed and examined. The analysis is done using computational programming in MATLAB (month: May and location: New Delhi). The parametric values of potable water (PW) and DC electric power outputs (EPO) have been figured for different values of mass flow rate (MFR), a number of collectors (*N*), packing factor (PF), and water depth (WD). Elaborative observation says that the value of PW output declines and DC EPO rises with the rise in MFR for the considered values of the number of collectors, EPO, and WD. Also, the values of DC electric power increases by 29.63% if PF is increased from 0.6 to 0.8 for the considered values of MFR, number of collectors, and water depth. Values of sensitivity figure with respect to *N* for PW yield and EPO have been found to be 0.303 and 0.992, respectively. Based on the results of all the analyses, sensible and effective conclusions are made.

Keywords: Sensitivity-analysis; PVT-FPC; Double slope solar still; Water depth

1. Introduction

The analysis of a solar desalination system consisting of solar collectors can provide one of the best alternatives for tackling the contemporary issue of shortage of freshwater around the globe. The sensitivity analysis (SA) of active solar distiller unit can be performed using one at a time (OAT) technique of SA for knowing the effect of variation of input parameters like mass flow rate (MFR), a number of collectors (*N*), packing factor (PF) and water depth (WD) on the outputs like potable water (PW) output and electric power output (EPO). The solar desalination technique of providing PW and energy is eco-friendly, maintenance-free, reliable, uses modest machinery, and can work individually in remote areas where sunlight is plentifully available. The vast range of applications of the current setup helps in the development of an eco-friendly atmosphere in the wide geographical coverage of the earth. It is the best-suited application for far-flung areas in developing or under developing countries both. The study says that, due to the unavailability of various natural resources, by 2025 two-third of the world's population will face a shortage of water

* Corresponding author.

as we on earth can access only less than 1% of the available water and that is also becoming polluted day by day due to various anthropogenic activities. The biggest challenge in the current scenario is the sustainable protection of drinking water. Also, the major challenge of both drought and flood are fatal and are being faced in different parts of the world. In the coming days, as reported by the UN, the quality of freshwater will be poor and non-drinkable.

The solar distiller units are either passive or active type distiller units. The passive unit does not take any heat from outside sources. It suffers from the problem of low distillate output and this drawback of passive unit is addressed in active solar distiller where an external source of heat is integrated with the basin of solar still to add heat to water in the basin thus results in increased temperature of the water surface in the basin and higher evaporation is obtained which leads to higher distillate output. At the outset, Rai and Tiwari [1] and Zaki et al. [2]) examined active solar distiller unit in the laboratory and performed various experimental analysis to identify the applications. Later, the continuous variations have been presented and published by various researchers and scientists for its design and analysis. Tiwari and Sahota [3] reviewed the elaborative operational behavior of a similar set-up and analyzed active solar distiller combined with the photovoltaic module and predicted its self-sustainable behavior. The results thus obtained by Tiwari and Sahota [3] helped a lot in identifying the gaps in the existing research on solar distiller. Kumar and Tiwari [4] also experimentally investigated such an active solar distiller unit and concluded that the combination enhances the production of PW by more than 3.5 times as compared to conventional solar distiller units. They made several experimental attempts and calibrated the results obtained as an average value of the number of iterations developed. Later, Tiwari et al. [5] and Singh et al. [6] analyzed the system by partially covering the series-connected flat plate collectors (FPCs) with photovoltaic thermal (PVT). Singh et al. [6] has made a great impact by analyzing the partially covered unit. The analysis reported was helpful in identifying the efficiencies of the combination. The results obtained say that though thermal efficiency is lower than the system reported by Kumar and Tiwari [4] the exergy efficiency and overall thermal efficiency values of the system are partially covered PVT-FPCs are better.

Issa and Chang [7] experimentally demonstrated the performance of solar still integrated with evacuated tubes for West Texas climatic condition and reported that the capacity of producing PW for the active system was 2.36 times higher than the passive system due to increased water temperature in the basin by approximately 20°C. Singh [8] examined single slope passive solar still and SS integrated with N identical partially covered (25%) PVT-FPCs and SS integrated with N identical PVT compound parabolic concentrator collectors (CPCs). The experimentation leads to the generation of several runtimes and human errors which were thus omitted during the analysis of partially covered distiller units. He clinched that the life cycle conversion efficiency of N-PVT-FPC-SS was higher by 56.25% and 37.5% than N-PVT-CPC-SS and single slope passive solar still respectively under optimized condition. The reason was attributed to the higher exergy output of N-PVT-FPC-SS under optimized conditions. In a study, it was reported that the life cycle conversion efficiency of evacuated tubular collector integrated solar still as compared to a similar passive system was higher due to higher exergy obtained from the active system. The positivity of results leads to the development of the optimized solar still [9]. Fathy et al. [10] concluded that the daily efficiency of double slope solar still with tracked parabolic trough collector was 29.86% when experimentally studied the performance of double slope solar still by integrating with parabolic trough collector.

Singh and Tiwari [11] developed an analytical characteristic equation for N identical evacuated tubular collectors integrated double slope solar still. Further, Kumar et al. [12] developed the analytical characteristic equation for single slope solar distiller coupled with N alike compound parabolic concentrator integrated evacuated tubular collectors and concluded that the performance of the reported system was better than the single slope solar distiller integrated with evacuated tubular collectors due to the increased heat collection area. Prasad et al. [13] performed the sensitivity analysis of double slope active solar still and concluded that the electric power output gets enhance marginally by 0.95% if the water depth is changed from 0.07 to 0.14 m for the selected values of MFR, N due to diminished solar cell temperature at higher water depth. Singh et al. [14] reported the effect of water mass on the performance of single slope solar still coupled with PVT-FPC and concluded that the enhancement in daily efficiency and productivity is significant till water depth of 1.4 m.

The literature survey suggests that the sensitive analysis of N number of collectors that are partly enclosed PVT-FPCs integrated double slope solar distiller has not been investigated and reported by any researcher around the globe. In the present work, the effect of variation of MFR, N and PF on PW output and electrical power output has been reported. The main objectives of the research study are as follows:

- To investigate the effect of variation of MFR on PW and EPO for the selected values of N, PF and WD for N-PVT-FPC-DS.
- To study the effect of change in the value of N on the PW and EPO for the selected values of MFR, PF and WD for the proposed system and also to plot the variation curves of the results obtained.
- To examine the effect of change of PF on outputs of the system for the considered values of MFR, WD and N for the system under operation. The results are plotted for systematic interpretations.
- To investigate the effect of change of WD on outputs (PW and EPO) of the proposed system for selected values of N, PF and MFR.

2. System description

The geometrical representation of series-connected N identical and partly covered PVT-FPCs integrated double slope solar distiller unit is shown in Fig. 1. The cross-sectional view of the first collector has been presented in Fig. 2 and XX′ view has been presented in Fig. 3. The values of various constraints are presented in Table 1. Wind

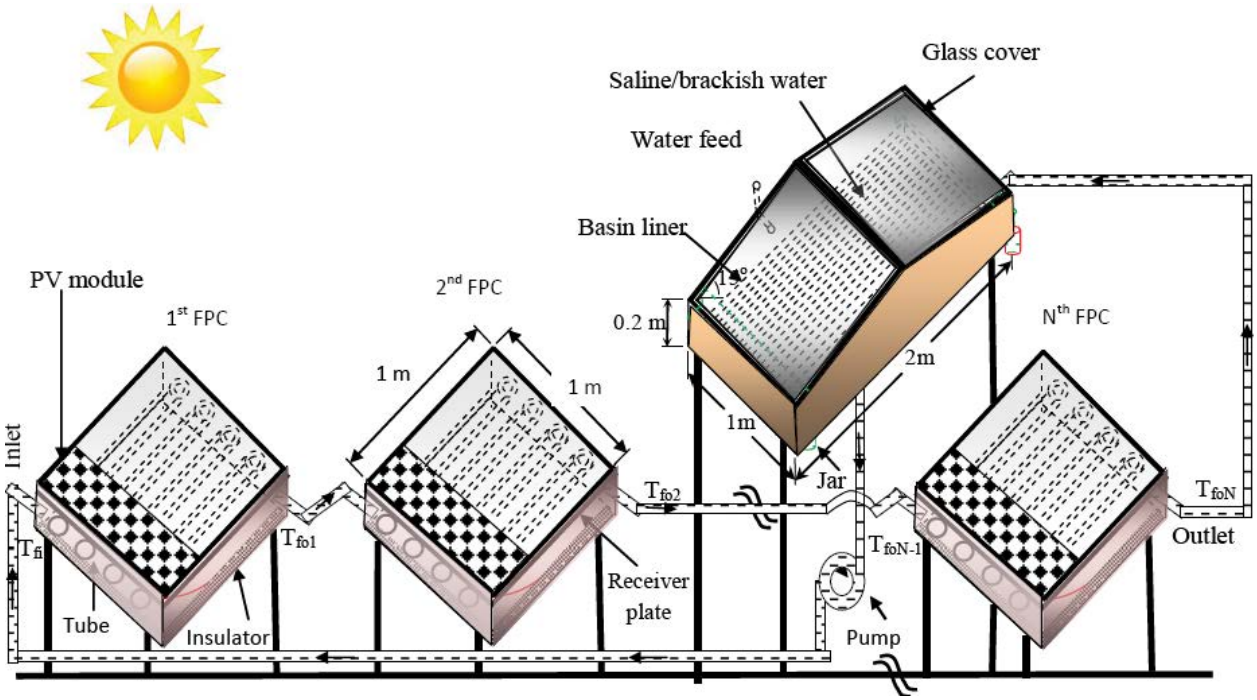

Fig. 1. *N* identical partially covered PVT-FPCs integrated double slope solar distiller unit.

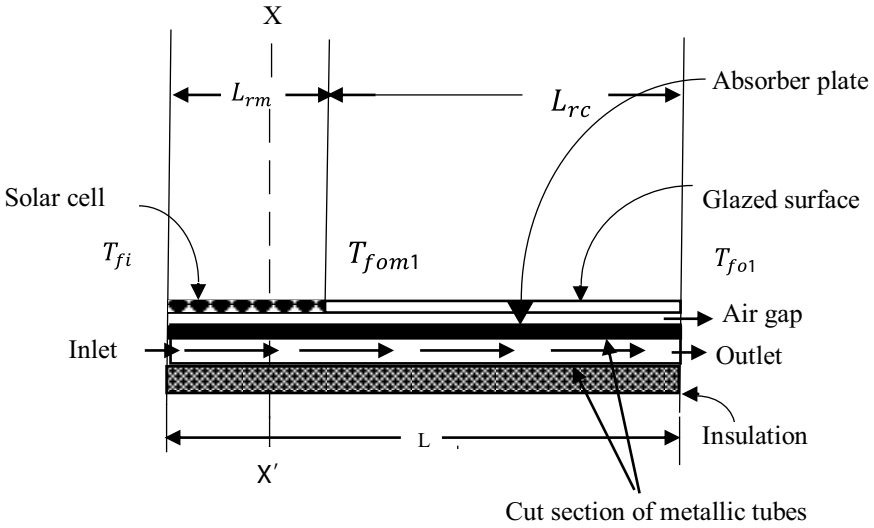

Fig. 2. The cross-section side view of the first part covered PVT-FPC.

velocity (average) during May 2019 is approximately 4.02 m/s. Here, for attaining a higher temperature of water at the outlet of the last collector, collectors are connected in series which helps to gain heat in the collectors, and thus hot water is obtained at the outlet of N^{th} collector for transferring heat to water kept in the basin. When solar flux falls on the surface of the condensing cover, it is transmitted to the water surface after reflection and absorption at the condensing surface. Again, the solar flux at the surface is first reflected, and then it is transmitted to the basin liner after absorption by water in the basin. The basin liner absorbs almost all solar flux and the temperature of basin lines increases which in turn transmits heat to water in the basin. In this way, water receives heat from collectors, direct sunlight falling on the surface and indirect heat from basin liner. Hence, the temperature of water in the basin rises and evaporation occurs which in turn gets condensed at the inner surface of the condensing cover. The film-wise condensation is ensured by proper cleaning the inside surface of the condensing cover and providing a slight inclination to the condensing surface. The condensed water at the inside surface of the condensing cover trickles down to the channel provided at the smaller wall and lastly, the condensed water is siphoned off from the channel.

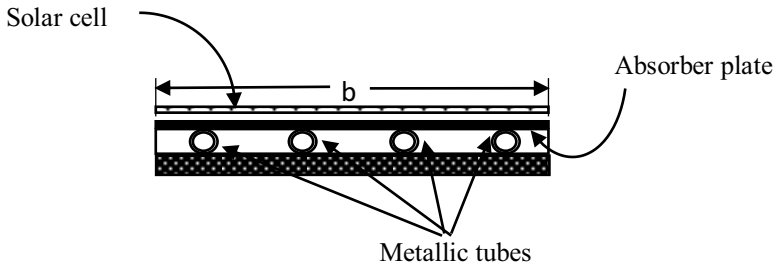

Fig. 3. Cut section XX′ front view of the first part covered PVT-FPC.

Table 1
Specifications of double slope solar still integrated with *N* identical partly covered photovoltaic thermal flat plate collectors

Component	Specification	Component	Specification
Double slope solar still			
Length	2 m	Orientation	East-West
Width	1 m	Thickness of glass cover	0.004 m
Inclination of glass cover	15°	*K*	0.816 W/m-K
Height of smaller side	0.2 m	Thickness of insulation	0.1 m
Material of body	GRP	Thermal conductivity of insulation	0.166 W/m-K
Material of stand	GI	ϵ_w	0.82
Cover material	Glass	ϵ_g	0.92
Partially covered PVT-FPC			
Type and no of collectors	Tube in plate type, *N*	Area of PV module	0.25 m × 1.0 m
Area of solar collector	1.0 m × 1.0 m	*F*′	0.968
Collector plate thickness	0.002 m	τ_g	0.95
Thickness of copper tubes	0.00056 m	α_c	0.9
Length of each copper tubes	1.0 m	β_c	0.89
Thickness of insulation	0.1 m	α_p	0.8
Angle of FPC with horizontal	30°	K_i	0.166 W/m-K
Thickness of toughened glass on FPC	0.004 m	FF	0.8
Effective area of collector under glass	0.25 m^2	Pipe diameter	0.0125 m
DC motor rating	12 V, 24 W		

3. Mathematical equations

Here, for getting mathematical equations for the system, energy balance equations (EBEs) are written for the different components of the system. These equations are then solved to obtain water and condensing cover/glass temperatures in terms of several known parameters such as solar flux, ambient air temperature, heat transfer coefficients (HTCs), etc taking assumptions the same as listed by Gupta et al. [15].

3.1. Determining useful heat gain (ṠuN) for N identical (series connected) partially covered PVT-FPCs

The useful heat gain from *N*-PVT-FPCs and temperature at the outlet of the last collector (N^{th} collector) can be written as [16,17]:

$$\dot{Q}_{u,N} = N\left(A_m + A_c\right)\left[\left(\alpha\tau\right)_{\text{eff},N} I\left(t\right) - U_{L,N}\left(T_{\text{fi}} - T_a\right)\right] \quad (1)$$

$$T_{\text{foN}} = \frac{\left(\text{AF}_R\left(\alpha\tau\right)\right)_1}{\dot{m}_f C_f}\frac{\left(1-K_k^N\right)}{\left(1-K_k\right)} I\left(t\right) + \frac{\left(\text{AF}_R U_L\right)_1}{\dot{m}_f C_f}\frac{\left(1-K_k^N\right)}{\left(1-K_k\right)} T_a + K_k^N T_{\text{fi}} \quad (2)$$

where T_{foN} stands for the temperature at the outlet of the last collector (N^{th} collector) and T_{fi} stands for the temperature at the inlet of the first collector. The variable T_{fi} can be taken as identical to T_w because water from the basin is compelled to go into the inlet of the first collector with the help of a pump due to the formation of a closed-loop with the basin. Also, heated water available at the outlet of the last collector (N^{th} collector) is made to flow to the basin of solar still. Hence, variable T_{wo} can be taken identical to T_{foN}. Various unknown terms in Eqs. (1) and (2) have been presented in Appendix-A.

The analytical expression for electrical efficiency [18,19] of solar cells (η_{cN}) of *N* identical PVT-FPC can be computed as:

$$\eta_{cN} = \eta_0\left[1-\beta_o\left(\overline{T}_{cN}-T_0\right)\right] \tag{3}$$

where η_0 stands for the efficiency at standard test condition. The emblem $\overline{T}_{cN}$ stands for the mean value of solar cell temperature of N^{th} collector and its value can be calculated using the relation reported by Shyam et al. [17] in which T_{fi} is identical to T_w as series-connected collectors have been put to form a closed loop with basin.

3.2. EBEs for double slope solar still

Following Dwivedi and Tiwari [20], energy balance equations for various components of *N*-PVT-FPC-DS can be written and they can be solved using Eq. (1) to get water temperature (T_w) and glass temperature (T_{giE}, T_{giW}, T_{goE} and T_{goW}) as follows.

$$T_w = \frac{\overline{f}_2(t)}{a_2}\left(1-e^{-a_2 t}\right)+T_{w0}e^{-a_2 t} \tag{4}$$

$$T_{giE} = \frac{A_1+A_2T_w}{P} \tag{5}$$

$$T_{giW} = \frac{B_1+B_2T_w}{P} \tag{6}$$

$$T_{goE} = \frac{\frac{K_g}{L_g}T_{giE}+h_{1gE}T_a}{\frac{K_g}{L_g}+h_{1gE}} \tag{7}$$

$$T_{goW} = \frac{\frac{K_g}{L_g}T_{giW}+h_{1gW}T_a}{\frac{K_g}{L_g}+h_{1gW}} \tag{8}$$

After evaluating the glass temperature from Eqs. (5)–(8) and water temperature from Eq. (4), one can obtain hourly yield for *N*-PVT-FPC-DS as follows:

$$\dot{m}_{ew} = \frac{h_{ewE}\frac{A_b}{2}\left(T_w-T_{giE}\right)+h_{ewW}\frac{A_b}{2}\left(T_w-T_{giW}\right)}{L}\times 3{,}600 \tag{9}$$

The evaporative heat transfer coefficient used in Eq. (9) can be evaluated with the help of the following equations:

$$h_{ewg} = 16.273\times10^{-3}h_{cwg}\left[\frac{P_w-P_{gi}}{T_w-T_{gi}}\right] \tag{10}$$

Here,

$$h_{cwg} = 0.884\left[\left(T_w-T_{gi}\right)+\frac{\left(P_w-P_{gi}\right)\left(T_w+273\right)}{\left(268.9\times10^3-P_w\right)}\right] \tag{11}$$

$$P_w = \exp\left[25.317-\frac{5{,}144}{\left(T_w+273\right)}\right] \tag{12}$$

$$P_{gi} = \exp\left[25.317-\frac{5{,}144}{\left(T_{gi}+273\right)}\right] \tag{13}$$

The different terms used in Eqs. (4)–(9) have been presented in Appendix-A. The value of hourly electrical energy or hourly electrical exergy can be computed as:

$$\dot{E}x_{elec} = A_m I(t)\sum_1^N\left(\beta_c\tau_g\eta_{cN}\right) \tag{14}$$

The daily electrical power can be computed by adding hourly electric power for 10 h because solar intensity exists for 10 h only.

3.3. Experimental validation of N alike FPCs integrated with double slope solar distiller unit

3.3.1. For N identical FPCs

Selmi et al. [21] performed the experimental validation of FPC taking $N = 1$ using the computational fluid dynamic concept. They considered the area of FPC as 0.249 m^2 diameter of copper tube as 0.5 inches. Data for different temperatures, solar intensity, and MFR were collected for a typical day in December 2004. They found a fair agreement between theoretical and experimental values of outlet temperature. Further, Rodríguez-Hidalgo et al. [22] performed the experimental validation of FPC having an area of 50 m^2 using a dynamic energy balance equation under the transient regime. Data for collector temperatures and heat loss were collected for a year from February 2008 to March 2009. They found a fair agreement between theoretical and experimental values.

3.3.2. For double slope solar distiller unit

An experimental validation of basin type double slope passive solar still has been done by Dwivedi and Tiwari [23] for New Delhi climatic condition at different water depths taking basin area as 2 m^2. Data for solar intensity, ambient air temperature, water temperature, condensing cover temperatures, and hourly yield were collected from October 2005 to September 2006. They evaluated heat transfer coefficients and hourly yield for April 2006 using various models namely Kumar and Tiwari [24], Dunkle [25], Adhikari et al. [26], Zheng et al. [27], and Clark [28]. The best result for the heat transfer coefficient and hourly yield was obtained using Dunkle's model. They found a fair agreement between experimental and theoretical values of hourly yield using Dunkle's model taking percentage error as the basis.

3.4. Sensitivity analysis

It aims at a deep understanding of the relationship between the input and output variables. There are many

techniques for conducting the SA; however, the simplest and most common approaches involve the changing parameters of variable/factor OAT to see what effect this produces on the output [21]. The notable point here is that only one variable is changed and the rest of all other variables are kept constant. This method of SA is appreciated as it helps the modeler to easily identify the input factor responsible for the model failure [22]. Fig. 4 presents the purification of saline/brackish water to PW using active solar still. The output and input variables have been shown. Out of the input variables, solar flux and ambient air temperature cannot be monitored as they are highly dependent on weather. Other variables can be monitored. So, the change in output with the change in one input (say MFR) while keeping all other inputs constant can be computed and plotted. A similar process can be applied to other parameters also.

4. Methodology

The succeeding stepwise methodology has been employed for the SA of DS having *N*-identical and partially covered PVT-FPCs with series connection:

- *Step I*: The initial data, that is, solar flux and the ambient air temperature for New Delhi's climatic conditions were obtained from IMD, Pune, India. Also for the inclined surface, Liu and Jordon's formula has been incorporated in the MATLAB to compute the scale of solar intensity at 30° northern latitude.
- *Step II*: Firstly, the magnitudes of T_w and T_{gi} are evaluated using Eqs. (5) and (6), respectively. Then the magnitude of hourly yield has been computed using Eq. (8). Later the values of hourly EPO were computed by Eq. (4) and the daily electric power output by the addition of hourly EPO for 10 h.
- *Step III*: Evaluate the values of hourly PW and daily EPO for various standards of one varying input parameter keeping all others as constant. Later the results obtained were 2D plotted.
- *Step IV*: Finally, step III has been repeated by varying all the input parameters one at a time except the ambient air temperature and solar intensity.

Fig. 5 represents the flow chart for a better understanding of the methodology followed for carrying out sensitivity analysis.

5. Results and discussion

Various input parameters have been fed in MATLAB for carrying out the SA of the projected system. The magnitude of solar flux and ambient air temperature can be obtained from Fig. 6 which has been taken from the Indian Meteorological Department, Pune, India. The output attained is presented in Figs. 7–26. All the parameters are analyzed using the OAT method only.

For the constants, N = 11, β_c = 0.89, and d = 0.14 m in Fig. 7, the per hour dissimilarity of PW output (yield) with MFR has been evaluated and plotted. It is seen from Fig. 7 that the hourly PW output falls as the value of MFR is increased. The reason identified is the improved quantity of water per unit time with increasing MFR and hence the lower increase in temperature is observed at the outlet of N^{th} collector. Also, it reduces the gap between two consecutive curves of PW output, and the curves may overlap if the MFR is continuously increasing. This is because the flowing fluid inside the tubes of collectors will get less time to absorb heat from the absorber plate with increased MFR and after a certain value of MFR a steady state will be achieved. At this state heat absorbed by water is approximately equal to the heat gained by the absorber plate. Here, it should be noted that an increase in MFR has a negative effect on PW output.

Fig. 8 shows the variation of daily PW output with MFR at given values of *N*, WD, and packing factor. It is seen from Fig. 8 that the value of yield decreases as the value of MFR is increased. It has been found to occur because fluid passing through tubes of collectors does not get sufficient time to absorb heat at an increased value of MFR and a comparative lesser rise in water temperature is obtained. Fig. 9 shows the variation of the percentage change in daily yield with the percentage change in MFR at given values of *N*, WD, and packing factor for double slope solar still integrated with *N* identical partially covered PVT-FPCs for a typical day in the month of May. The slope of this curve gives the sensitivity figure for PW output with respect to MFR. The average value of the sensitivity figure for PW yield with respect to MFR has been found to be 0.121.

For the constants $\dot{m}_f$ = 0.03 kg/s, β_c = 0.89 and d = 0.14 m, Fig. 10 characterizes the deviation of hourly PW output with *N* (number of collectors). Fig. 7 shows that the value of PW output increases with the increasing value of *N* because heat added to the water kept in the basin also increases and with the increase in heat added to the water, the evaporation of water also increases, therefore with an increase in the value of *N* we get higher magnitudes of PW output. Also, the rise in the value of *N* results in the decrease in the gap between two consecutive hourly PW output curves. For example, the gap between PW output curves for *N* = 10 and *N* = 12 is less than the gap between PW output curves for *N* = 2 and *N* = 4. On further increasing the values of *N*, the PW output curves either overlaps

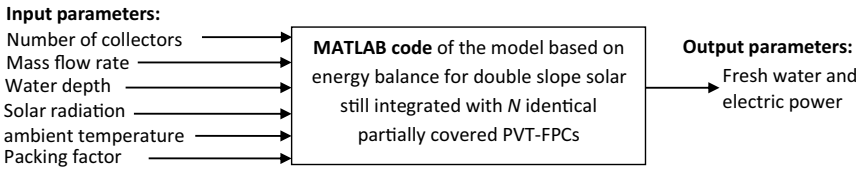

Fig. 4. Purification of saline/brackish water to potable water using PVT-FPCs integrated double slope solar distiller.

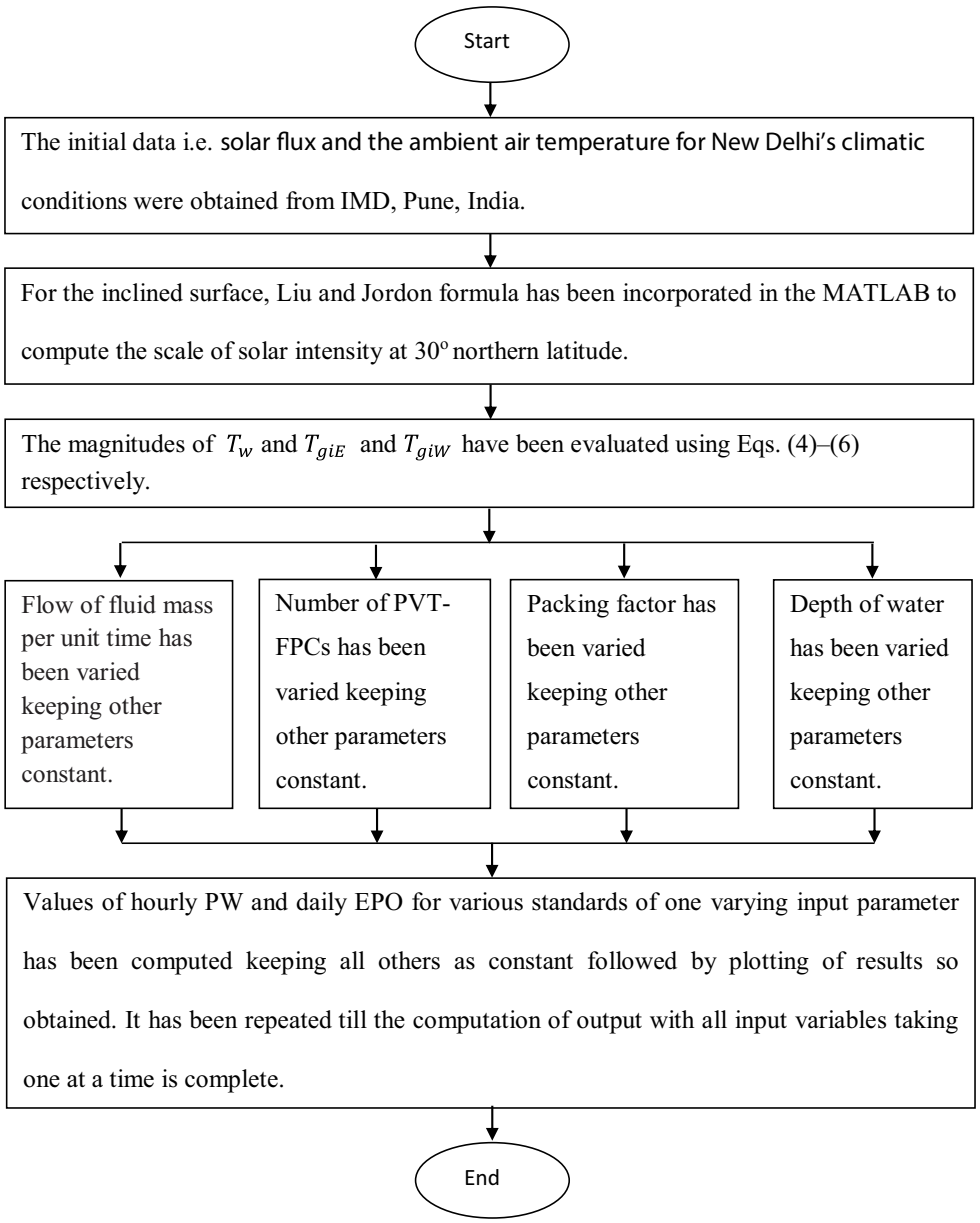

Fig. 5. Flow chart representing the methodology followed for carrying out sensitivity analysis.

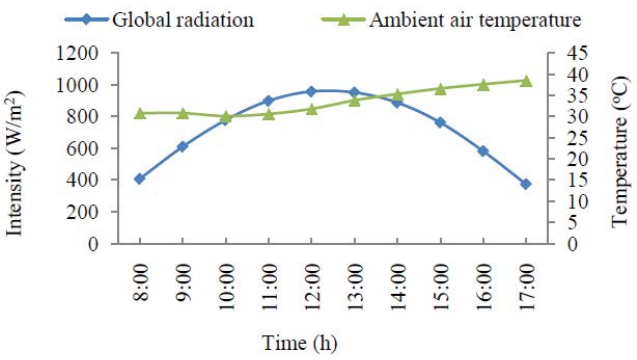

Fig. 6. Hourly variation of intensity and ambient air temperature for a typical day in the month of May.

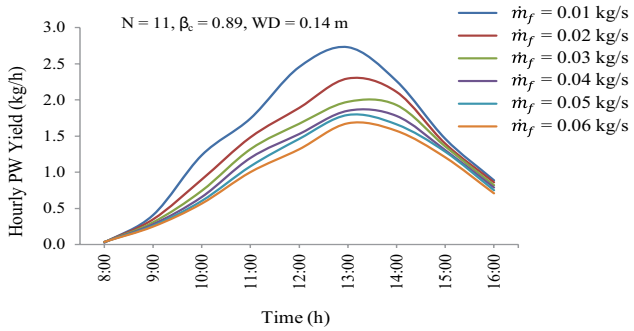

Fig. 7. Variation of hourly yield with mass flow rate for double slope solar still integrated with N identical partially covered PVT-FPCs for a typical day in the month of May.

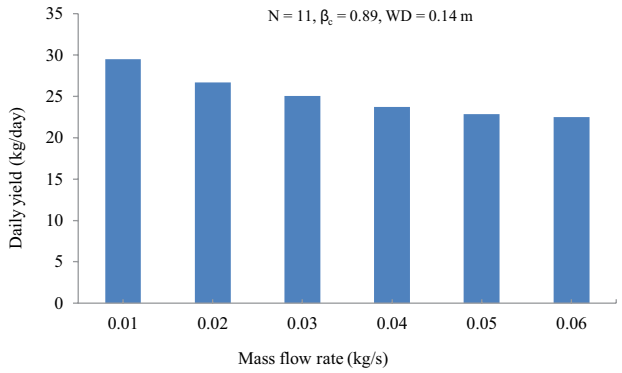

Fig. 8. Variation of daily yield with mass flow rate for double slope solar still integrated with N identical partially covered PVT-FPCs for a typical day in the month of May.

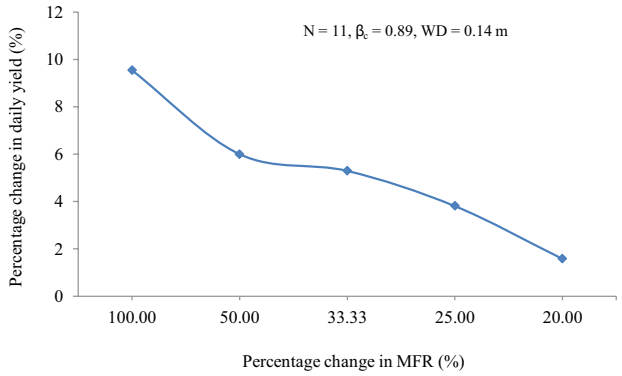

Fig. 9. Variation of the percentage change in daily yield with the percentage change in MFR for double slope solar still integrated with N identical partially covered PVT-FPCs for a typical day in the month of May (SA).

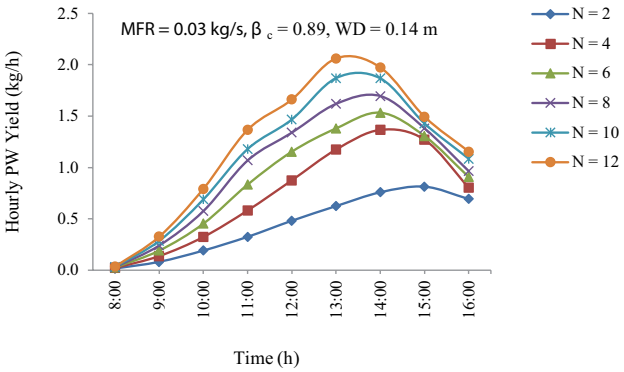

Fig. 10. Variation of hourly yield with a number of collectors (N) for double slope solar still integrated with N identical partially covered PVT-FPCs for a typical day in the month of May.

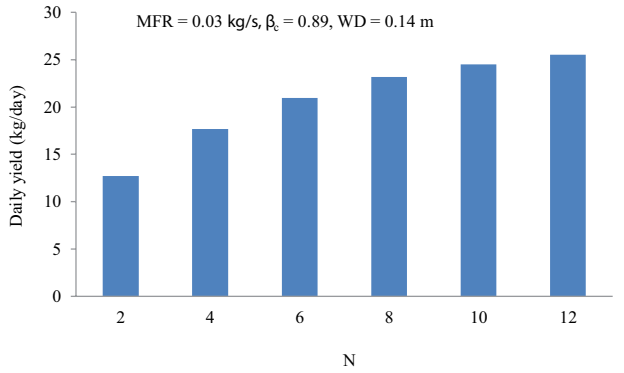

Fig. 11. Variation of daily PW yield with N for double slope solar still integrated with N identical partially covered PVT-FPCs for a typical day in the month of May.

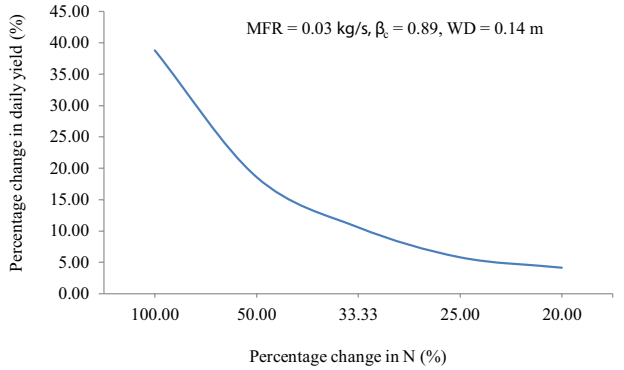

Fig. 12. Variation of the percentage change in daily yield with the percentage change in N for double slope solar still integrated with N identical partially covered PVT-FPCs for a typical day in the month of May (SA).

or we get insignificant output, above 100°C, the thermal model becomes invalid. So, for economical PW output, the value of N should be selected such that water temperature is below the boiling point of water.

Fig. 11 represents the variation of daily PW yield with N at given values of MFR, WD, and packing factor for double slope solar still integrated with N identical partially covered PVT-FPCs for a typical day in the month of May. It is observed from Fig. 11 that the value of PW yield increases as the value of N increases due to the increased amount of heat added to the basin. Fig. 12 represents the variation of the percentage change in daily yield with the percentage change in N at given values of MFR, PW, and packing factor for double slope solar still integrated with N identical partially covered PVT-FPCs for a typical day in the month of May. The slope of the curve in Fig. 12 represents the sensitivity figure of PW yield with respect to N. The average value of the sensitivity figure of PW yield with N has been evaluated to be 0.303.

Now, for the constants, $\dot{m}_f$ = 0.03 kg/s, N = 11 and d = 0.14 m, Fig. 13 represents the variation of hourly PW output with PF of PVT. Results show that the PW output decreases as PF is increased. Also, the amount of solar flux reaching the water flowing through tubes of the collector is less with increased PF, which results in less increase in the value of the temperature of water at the outlet of N^{th} collector. Hence, we get lower evaporation and therefore lower PW output.

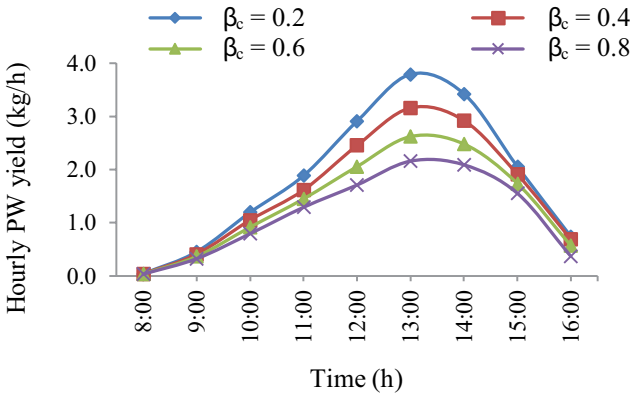

Fig. 13. Variation of hourly yield with packing factor (β_c) for double slope solar still integrated with N identical partially covered PVT-FPCs for a typical day in the month of May.

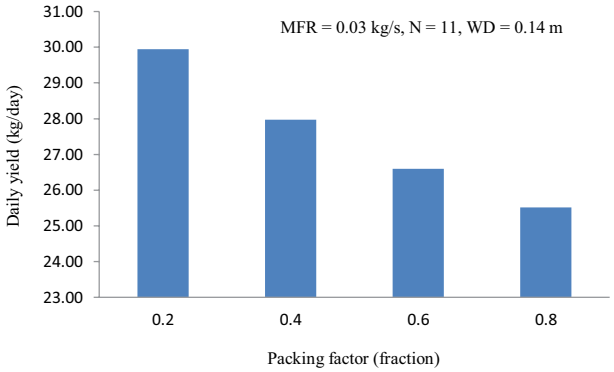

Fig. 14. Variation of daily yield with packing factor (β_c) for double slope solar still integrated with N identical partially covered PVT-FPCs for a typical day in the month of May.

Fig. 14 represents the variation of daily yield with packing factor at given values of N, MFR, and WD for double slope solar still integrated with N identical partially covered PVT-FPCs for a typical day in the month of May. It is seen from Fig. 14 that the value of the daily PW yield decreases as the value of the packing factor is increased. It has been found to occur because more area of collector gets covered by PVT as the value of packing factor increases which result in less addition of heat to water flowing through the collector. It results in less rise in temperature of water in the basin and hence decreased PW yield is obtained. Fig. 15 represents the variation of the percentage change in daily yield with the percentage change in packing factor at given values of MFR, N, and WD for double slope solar still integrated with N identical partially covered PVT-FPCs for a typical day in the month of May. The slope of the graph in Fig. 15 represents the sensitivity figure for PW yield with respect to the packing factor. The average value of the sensitivity figure for PW yield with respect to the packing factor has been found to be 0.095.

Keeping the constants, N = 11, $\dot{m}_f$ = 0.03 kg/s and β_c = 0.89, Fig. 16 represents the variation of hourly PW output with WD. Multiple computations were performed. The results obtained say that during sunshine the value of PW output has been found to decrease as WD increases. This is because of the higher quantity of water in the basin of the system for the same amount of heat added. So, a higher amount of water lowers the rise in temperature of water in the basin and hence lowers the evaporation, finally resulting in lower distillate output.

Fig. 17 represents the variation of daily yield with WD at given values of MFR, N, and packing factor for double slope solar still integrated with N identical partially covered PVT-FPCs for a typical day in the month of May. It has been observed from Fig. 17 that the value of PW yield increases as the value of WD increases due to the increased value of heat content of water mass at an increased value of WD. Actually, PW yield during day time decreases with the increase in water depth as usual which happens due to higher heat absorption by water mass in the basin at increased water mass in the basin at higher WD. Fig. 18 shows the variation of the percentage change in daily PW

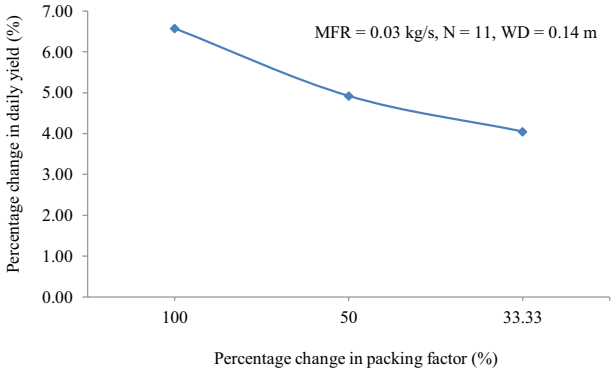

Fig. 15. Variation of the percentage change in daily yield with the percentage change in packing factor for double slope solar still integrated with N identical partially covered PVT-FPCs for a typical day in the month of May (SA).

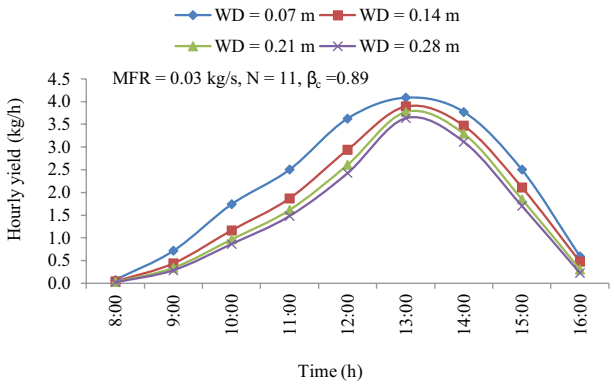

Fig. 16. Variation of hourly PW yield with WD for double slope solar still integrated with N identical partially covered PVT-FPCs for a typical day in the month of May.

yield with the percentage change in WD at given values of MFR, N and packing factor for double slope solar still integrated with N identical partially covered PVT-FPCs for a typical day in the month of May. The slope of the curve

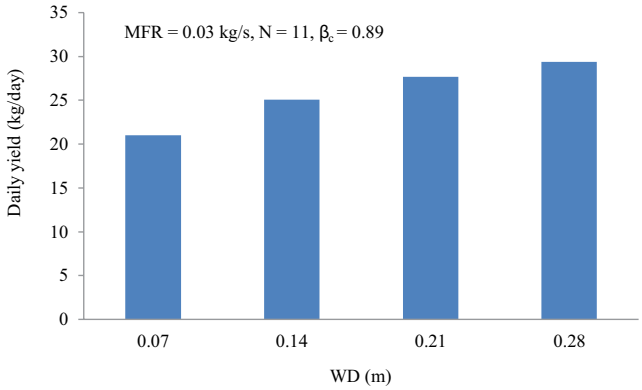

Fig. 17. Variation of daily yield with WD for double slope solar still integrated with *N* identical partially covered PVT-FPCs for a typical day in the month of May.

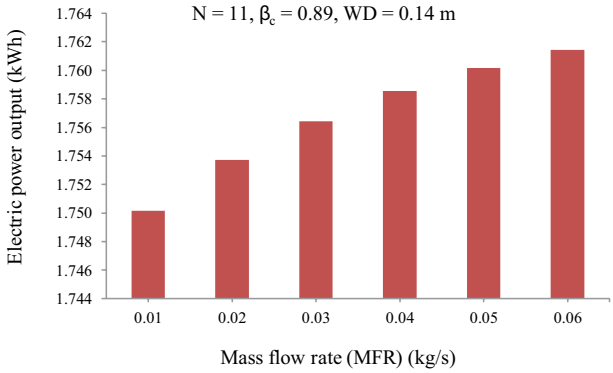

Fig. 19. Variation of daily electric power output with a mass flow rate for double slope solar still integrated with *N* identical partially covered PVT-FPCs for a typical day in the month of May.

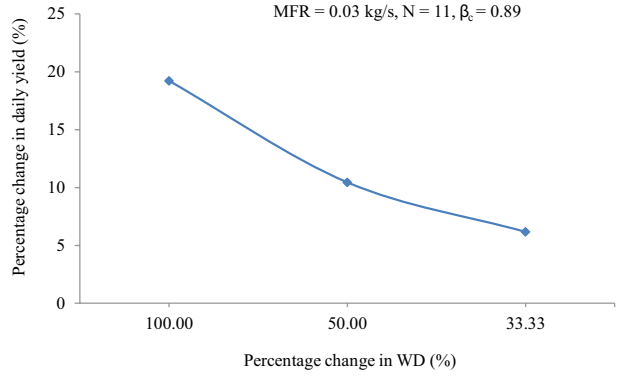

Fig. 18. Variation of the percentage change in daily yield with the percentage change in WD for double slope solar still integrated with *N* identical partially covered PVT-FPCs for a typical day in the month of May (SA).

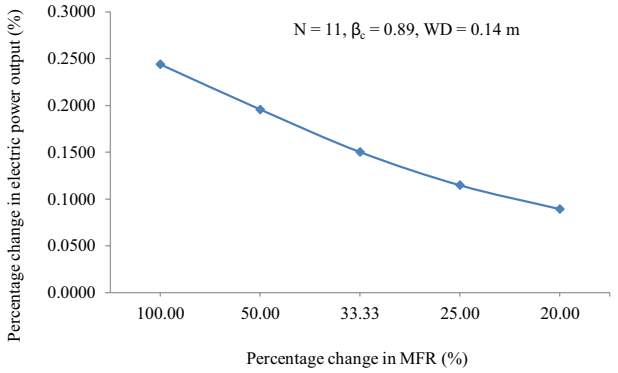

Fig. 20. Variation of the percentage change in daily electric power output with the percentage change in MFR for double slope solar still integrated with *N* identical partially covered PVT-FPCs for a typical day in the month of May (SA).

in Fig. 18 indicates the value of the sensitivity figure for PW yield with respect to WD. The average value of the sensitivity figure for PW yield with respect to WD has been found to be 0.195.

For the constants N = 11, β_c = 0.89 and WD = 0.14 m, Fig. 19 showcases the dissimilarity of daily DC EPO with the variation in MFR. Results say that the magnitude of DC EPO rises as the magnitude of MFR is raised. The point to be noted here is that DC EPO increases due to the decreased temperature of a solar cell with raised MFR. Higher MFR means the higher velocity of flow of fluid flowing below PVT which results in an increased rate of heat transfer from the solar cell to the fluid. It is also observed that the increase in DC EPO is less at higher values of MFR. So the compromise is to be made between the PW output and DC EPO while selecting the MFR of any fluid. If the main aim is to get PW, a lower value should be preferred. At the same time, if the main aim is to get DC EPO, a higher value of MFR should be preferred. Fig. 20 represents the variation of the percentage change in daily electric power output with the percentage change in MFR at given values of *N*, WD, and packing factor for double slope solar still integrated with *N* identical partially covered PVT-FPCs for a typical day in the month of May. The slope of the curve in Fig. 20 indicates the value of the sensitivity figure for electric power output with respect to MFR. The average value of the sensitivity figure for electric power output with respect to MFR has been found to be 0.0040. For the constants, $\dot{m}_f$ = 0.03 kg/s, β_c = 0.89 and WD = 0.14 m, Fig. 21 characterizes the deviation of hourly DC EPO with *N*. For the given constant parameters, the obtained results show the increase in the magnitude of DC EPO with increasing value of *N* (as the area of the photovoltaic module also increases) and higher amount of solar flux is converted into electric power. An increase in *N* also leads to an increase in water temperature (above 100°C also). Therefore, the value of *N* should be selected in such a way that the temperature of the water is less than the boiling temperature of water for effective thermal modeling. As already mentioned; the water temperature above the boiling point (i.e., 100°C) is not acceptable and effective for thermal modeling. Thus, the selection of the value of *N* should be optimum. Fig. 22 shows the variation of the percentage change in daily electric power output with the percentage change in *N* for double slope solar still integrated with *N* identical partially

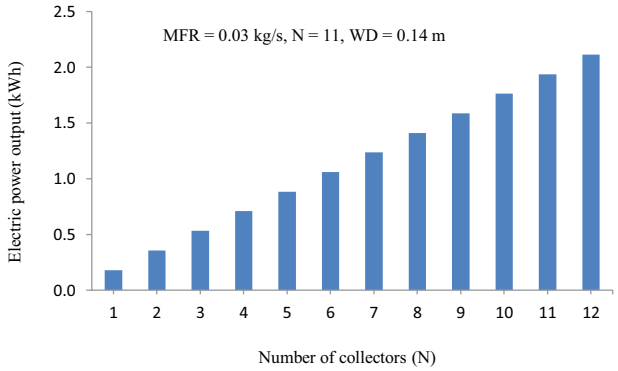

Fig. 21. Variation of daily electric power output with the number of collectors (*N*) for double slope solar still integrated with *N* identical partially covered PVT-FPCs for a typical day in the month of May.

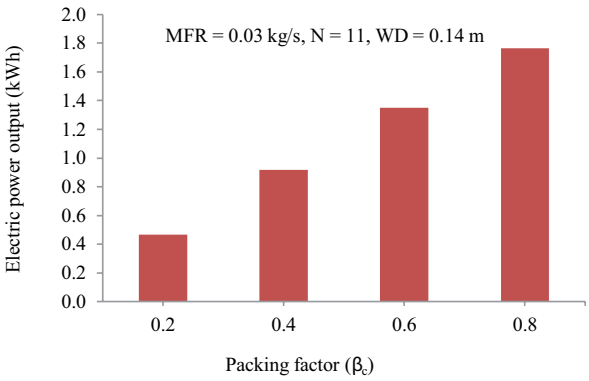

Fig. 23. Variation of daily electric power output with packing factor for double slope solar still integrated with *N* identical partially covered PVT-FPCs for a typical day in the month of May.

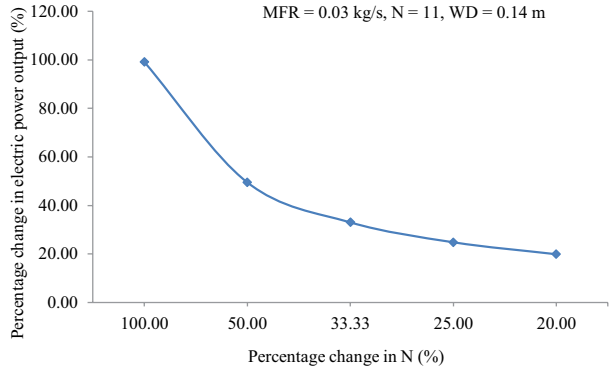

Fig. 22. Variation of the percentage change in daily electric power output with the percentage change in *N* for double slope solar still integrated with *N* identical partially covered PVT-FPCs for a typical day in the month of May (SA).

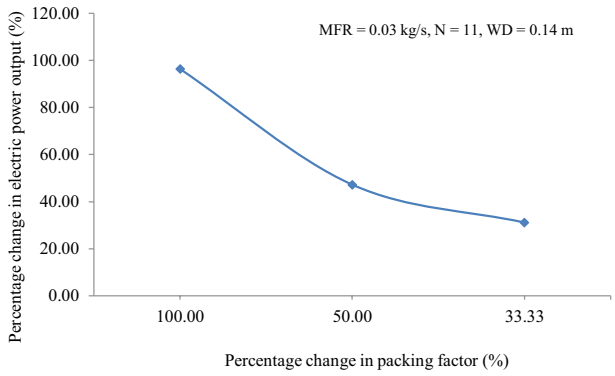

Fig. 24. Variation of the percentage change in daily electric power output with the percentage change in packing factor for double slope solar still integrated with *N* identical partially covered PVT-FPCs for a typical day in the month of May (SA).

covered PVT-FPCs for a typical day in the month of May. The slope of the curve in Fig. 22 indicates the value of the sensitivity figure for electric power output with respect to *N*. The average value of the sensitivity figure for electric power output with respect to *N* has been found to be 0.9919.

Also for the constants, $\dot{m}_f$ = 0.03 kg/s, *N* = 11 and WD = 0.14 m, Fig. 23 represents the variation of hourly DC EPO with EPO. It is observed that the value of DC EPO rises with the rise in the value of EPO for the given area and hence higher amount of solar flux is converted into electric power. Figs. 6 and 10 depict the relation between PW output, DC EPO, and MFR values. Fig. 6 clearly shows the negative effect on PW output with an increase in MFR values whereas Fig. 10 shows the positive effect on the EPO on the desired magnitudes of MFR. Hence, one has to make a compromise between PW output and DC EPO while selecting the value of MFR. If PW output is the main product and DC EPO is the by-product, a lower value of MFR should be preferred and vice-versa. Therefore, based on the requirements and priority of the application, one can select the MFR values to get optimum/desired outputs. Fig. 24 shows the variation of the percentage change in daily electric power output with the percentage change in packing factor at given values of MFR, *N*, and WD for double slope solar still integrated with *N* identical partially covered PVT-FPCs for a typical day in the month of May. The slope of the curve in Fig. 24 indicates the value of the sensitivity figure for electric power output with respect to the packing factor. The average value of the sensitivity figure for electric power output with respect to the packing factor has been found to be 0.9471.

Keeping the constants, *N* = 12, $\dot{m}_f$ = 0.03 kg/s and β_c = 0.89, Fig. 14 shows the dissimilarity in daily DC EPO with WD. Here the depth of water is the varying parameter. The output says, due to low water temperature in the basin, the value of daily DC EPO rises as a higher amount of heat will be taken away by water at higher WD. This allows passing through tube kept below PVT resulting in an amplified heat transfer rate. The amplification in the heat transfer was directly proportional to the depth of water in the setup and also DC EPO. Hence, a higher depth should be preferred. Fig. 26 shows the variation of the percentage change in daily electric power output with the percentage change in WD at given values of *N*, MFR, and packing factor for double slope solar still integrated with *N* identical partially

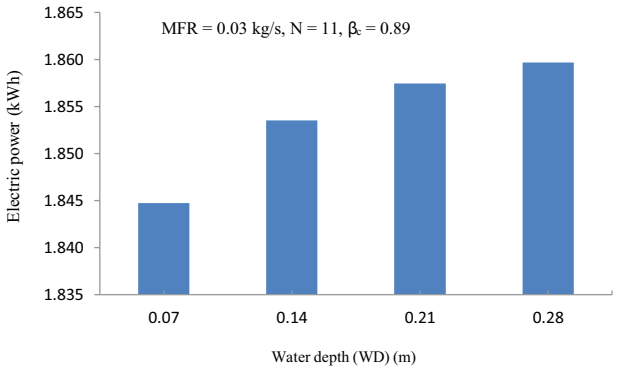

Fig. 25. Variation of daily electric power output with packing factor for double slope solar still integrated with *N* identical partially covered PVT-FPCs for a typical day in the month of May.

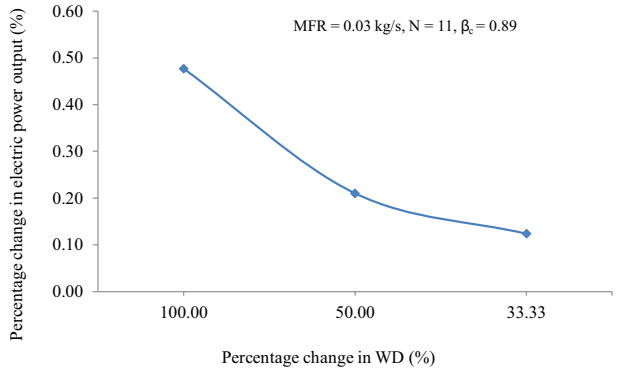

Fig. 26. Variation of the percentage change in daily electric power output with the percentage change in packing factor for double slope solar still integrated with *N* identical partially covered PVT-FPCs for a typical day in the month of May (SA).

covered PVT-FPCs for a typical day in the month of May. The slope of the curve in Fig. 24 indicates the value of the sensitivity figure for electric power output with respect to WD. The average value of the sensitivity figure for electric power output with respect to WD has been found to be 0.0042.

Table 2 shows the value of the sensitivity figure for *N* identical partly covered PVT-FPCs integrated double slope solar distiller. The sensitivity figure represents the significance of one output with respect to one input while keeping other parameters constant. It is observed from Table 2 that the value of sensitivity figure for both PW yield as well as electric power output is highest with respect to *N*. It means that the designer should pay the highest attention to the selection of *N* while designing and installing an active solar distiller. Further, it is observed that the packing factor is least significant from the PW yield viewpoint and MFR is the least significant from the electric power output viewpoint.

6. Conclusions

The sensitivity analysis for *N* identical partially covered PVT-FPCs integrated solar distiller unit has been carried out.

Table 2
Sensitivity analysis for *N* identical partly covered photovoltaic thermal flat plate collectors integrated double slope solar distiller

Parameter	Sensitivity figure
Average value of sensitivity figure for PW yield	
With respect to MFR	0.121
With respect to *N*	0.303
With respect to packing factor	0.095
With respect to WD	0.195
Average value of sensitivity figure for electric power output	
With respect to MFR	0.0040
With respect to *N*	0.9919
With respect to packing factor	0.9471
With respect to WD	0.0042

Based on the present research study, the following conclusions have been drawn:

- For the fixed values of *N*, PF and the depth of water; with increasing MFR, the value of PW output decreases and that of EPO increases.
- In the same setup, for the fixed values of MFR, PF and the depth of water, the rise in the value *N* leads to raising the values of both PW and DC EPO. However, while selecting the value of *N* during design and installation phases, one needs to maintain the water temperature below the boiling point of fluid (water) in the basin as well as in the tubes of water collectors.
- Again for the fixed values of *N*, MFR and WD, increasing the value of PF decreases the value of PW output; but, increases the value of DC EPO. So, during the design stage, a compromise between PW output and EPO is to be made while selecting the values of the EPO.
- The DC EPO has been found to increase with the increase in WD for the considered values of *N*, MFR and PF. However, hourly PW yield during sunshine hours has been found to decrease with the increase in WD. Hence, higher values of WD should be preferred if the main objective is to get higher EPO.
- The average value of sensitivity figure for both PW yield as well as electric power output has been found to be highest with respect to *N*. So, the value of *N* should be selected carefully while designing and installing an active solar distiller unit.

Symbols

A_b	—	Area of the basin, m^2
A_g	—	Area of the glass cover, m^2
C	—	Specific heat capacity, J/kg-K
DS	—	Double slope solar still
EPO	—	Electric power output
FF	—	Fill factor, dimensionless
F'	—	Collector efficiency factor, dimensionless
FPC	—	Flat plate collector
HTC	—	Heat transfer coefficient

h_{cwgE} — Convective HTC from water to the inner surface of glass cover facing east, W/m²-K
h_{cwgW} — Convective HTC from water to the inner surface of glass cover facing west, W/m²-K
h_{ewgE} — Evaporative HTC from the water surface to the inner surface of glass cover facing east, W/m²-K
h_{ewgW} — Evaporative HTC from the water surface to the inner surface of glass cover facing west, W/m²-K
h_{ba} — HTC from the blackened surface to water mass, W/m²-K
h_{bw} — HTC from the blackened surface to water mass, W/m²-K
h_{rwgE} — Radiative HTC from the water surface to the inner surface of glass cover facing east, W/m²-K
h_{rwgW} — Radiative HTC from the water surface to the inner surface of glass cover facing west, W/m²-K
h_r — Radiative HTC, W/m²-K
h_{1wE} — Total HTC from the water surface to inner surface of glass cover facing east, W/m²-K
h_{1wW} — Total HTC from the water surface to inner surface of glass cover facing west, W/m²-K
h_{1gE} — Total HTC from the outer surface of glass cover facing east to ambient, W/m²-K
h_{1gW} — Total HTC from the outer surface of glass cover facing west to ambient, W/m²-K
$I(t)$ — Solar intensity on the collector, W/m²
$I_{SE}(t)$ — Solar intensity on glass cover facing east, W/m²
$I_{SW}(t)$ — Solar intensity on glass cover facing west, W/m²
i — Rate of interest
K — Thermal conductivity, W/m-K
L_g — Thickness of glass, m
L — Latent heat, J/kg
L' — Length, m
MFR/$\dot{m}_f$ — Mass flow rate of fluid/water, kg/s
$\dot{m}_{ew}$ — Mass of distillate per hour from *N*-PVT-FPC-DS, kg
N — Number of collectors
PVT — Photovoltaic thermal
PF — Packing factor
PF_c — Penalty factor due to the glass covers for the glazed portion
PF_1 — Penalty factor first, dimensionless
PF_2 — Penalty factor second, dimensionless
PW — Potable water
SA — Sensitivity analysis
T_{foN} — Outlet water temperature at the end of the N^{th} water collector, °C
T_a — Ambient air temperature, °C
T_{giE} — Glass temperature at the inner surface of glass cover facing east, °C
T_{giW} — Glass temperature at the inner surface of glass cover facing west, °C
T — Time, h
T_{wo} — Water temperature at t = 0, °C
T_w — Water temperature, °C
U_L — Overall heat transfer coefficient
V — Velocity of air, m/s
WD — Water depth

Subscript

eff — Effective
en — Energy
ex — Exergy
f — Fluid
g — Glass
in — Incoming
out — Outgoing
w — Water
E — East
W — West

Greek

α — Absorptivity, fraction
η — Efficiency, %
$(\alpha\tau)_{eff}$ — Product of effective absorptivity and transmissivity
σ — Stefan – Boltzmann constant, W/m²-K⁴
τ — Transmittivity

References

[1] S.N. Rai, G.N. Tiwari, Single basin solar still coupled with flat plate collector, Energy Convers. Manage., 23 (1983) 145–149.
[2] G.M. Zaki, T. El Dali, H. El Shafie, Improved Performance of Solar Still, Proc., First Arab International Solar Energy Conference, Kuwait, 1983, pp. 331–335.
[3] G.N. Tiwari, L. Sahota, Advanced Solar-Distillation Systems: Basic Principles, Thermal Modeling, and Its Application, Springer, Singapore, 2017.
[4] S. Kumar, A. Tiwari, Design, fabrication and performance of a hybrid photovoltaic/thermal (PV/T) active solar still, Energy Convers. Manage., 51 (2010) 1219–1229.
[5] G.N. Tiwari, J.K. Yadav, D.B. Singh, I.M. Al-Helal, A.M. Abdel-Ghany, Exergoeconomic and enviroeconomic analyses of partially covered photovoltaic flat plate collector active solar distillation system, Desalination, 367 (2015) 186–196.
[6] D.B. Singh, J.K. Yadav, V.K. Dwivedi, S. Kumar, G.N. Tiwari, I.M. Al-Helal, Experimental studies of active solar still integrated with two hybrid PVT collectors, Sol. Energy, 30 (2016) 207–223.
[7] R.J. Issa, B. Chang, Performance study on evacuated tubular collector coupled solar still in West Texas climate, Int. J. Green Energy, 14 (2017) 793–800.
[8] D.B. Singh, Improving the performance of single slope solar still by including *N* identical PVT collectors, Appl. Therm. Eng., 131 (2018) 167–179.
[9] D.B. Singh, Energy metrics analysis of *N* identical evacuated tubular collectors integrated single slope solar still, Energy, 148 (2018) 546–560.
[10] M. Fathy, H. Hassan, M.S. Ahmed, Experimental study on the effect of coupling parabolic trough collector with double slope solar still on its performance, Sol. Energy, 163 (2018) 54–61.
[11] D.B. Singh, G.N. Tiwari, Analytical characteristic equation of *N* identical evacuated tubular collectors integrated double slope solar still, J. Sol. Energy Eng. ASME, 135 (2017) 051003 (1–11), https://doi.org/10.1115/1.4036855.
[12] R. Kumar, R. Sharma, D. Kumar, A.R. Singh, D.B. Singh, G.N. Tiwari, Characteristic equation development for single-slope solar distiller unit augmented with *N* identical parabolic concentrator integrated evacuated tubular collectors, J. Sol. Energy Eng. ASME, 142 (2020) 021011 (1–11), https://doi.org/10.1115/1.4045314.

[13] H. Prasad, P. Kumar, R.K. Yadav, A. Mallick, N. Kumar, D.B. Singh, Sensitivity analysis of *N* identical partially covered (50%) PVT compound parabolic concentrator collectors integrated double slope solar distiller unit, Desal. Water Treat., 153 (2019) 54–64.
[14] D.B. Singh, N. Kumar, Harender, S. Kumar, S.K. Sharma, A. Mallick, Effect of depth of water on various efficiencies and productivity of *N* identical partially covered PVT collectors incorporated single slope solar distiller unit, Desal. Water Treat., 138 (2019) 99–112.
[15] V.S. Gupta, D.B. Singh, R.K. Mishra, S.K. Sharma, G.N. Tiwari, Development of characteristic equations for PVT-CPC active solar distillation system, Desalination, 445 (2018) 266–279.
[16] S. Dubey, G.N. Tiwari, Analysis of PV/T flat plate water collectors connected in series, Sol. Energy, 83 (2009) 1485–1498.
[17] Shyam, G.N. Tiwari, I.M. Al-Helal, Analytical expression of temperature dependent electrical efficiency of *N*-PVT water collectors connected in series, Sol. Energy, 114 (2015) 61–76.
[18] D.L. Evans, Simplified method for predicting photovoltaic array output, Sol. Energy, 27 (1981) 555–560.
[19] T. Schott, Operational Temperatures of PV Modules, Proceedings of 6th PV Solar Energy Conference, 1985, pp. 392–396.
[20] V.K. Dwivedi, G.N. Tiwari, Experimental validation of thermal model of a double slope active solar still under natural circulation mode, Desalination, 250 (2009) 49–55.
[21] M. Selmi, M.J. Al-Khawaja, A. Marafia, Validation of CFD simulation for flat plate solar energy collector, Renewable Energy, 33 (2007) 383–387.
[22] M.C. Rodríguez-Hidalgo, P.A. Rodríguez-Aumente, A. Lecuona, G.L. Gutiérrez-Urueta, R. Ventas, Flat plate thermal solar collector efficiency: transient behavior under working conditions. Part I: model description and experimental validation, Appl. Therm. Eng., 31 (2011) 2394–2404.
[23] V.K. Dwivedi, G.N. Tiwari, Comparison of internal heat transfer coefficients in passive solar stills by different thermal models: an experimental validation, Desalination, 246 (2009) 304–318.
[24] S. Kumar, G.N. Tiwari, Estimation of convective mass transfer in solar distillation systems, Sol. Energy, 57 (1996) 459–464.
[25] R.V. Dunkle, Solar Water Distillation: The Roof Type Still and a Multiple Effect Diffusion Still, International Developments in Heat Transfer, ASME, University of Colorado, 1961, pp. 895–902.
[26] R.S. Adhikari, A. Kumar, A. Kumar, Estimation of mass-transfer rates in solar stills, Int. J. Energy Res., 14 (1990) 737–744.
[27] H.F. Zheng, X.Y. Zhang, J. Zhang, Y.Y. Wu, A group of improved heat and mass transfer correlations in solar stills, Energy Convers. Manage., 43 (2001) 2469–2478.
[28] J.A. Clark, The steady-state performance of a solar still, Sol. Energy, 44 (1990) 43–49.

Appendix-A

Expressions for various terms used in Eqs. (1) and (2) are as follows.

$$U_{\text{tca}} = \left[\frac{1}{h_o} + \frac{L_g}{K_g}\right]^{-1};\ U_{\text{tcp}} = \left[\frac{1}{h_i} + \frac{L_g}{K_g}\right]^{-1};$$

$$h_o = 5.7 + 3.8\,V,\ \text{Wm}^{-2}\text{K}^{-1};\ h_i = 5.7,\ \text{Wm}^{-2}\text{K}^{-1};$$

$$U_{\text{tpa}} = \left[\frac{1}{U_{\text{tca}}} + \frac{1}{U_{\text{tcp}}}\right]^{-1} + \left[\frac{1}{h_i'} + \frac{1}{h_{\text{pf}}} + \frac{L_i}{K_i}\right]^{-1};$$

$$h_i' = 2.8 + 3\,V,\ \text{Wm}^{-2}\text{K}^{-1};$$

$$U_{L1} = \frac{U_{\text{tcp}}U_{\text{tca}}}{U_{\text{tcp}} + U_{\text{tca}}};\quad U_{L2} = U_{L1} + U_{\text{tpa}};$$

$$U_{\text{Lm}} = \frac{h_{\text{pf}}U_{L2}}{F'h_{\text{pf}} + U_{L2}};\quad U_{\text{Lc}} = \frac{h_{\text{pf}}U_{\text{tpa}}}{F'h_{\text{pf}} + U_{\text{tpa}}};$$

$$\text{PF}_1 = \frac{U_{\text{tcp}}}{U_{\text{tcp}} + U_{\text{tca}}};\quad \text{PF}_2 = \frac{h_{\text{pf}}}{F'h_{\text{pf}} + U_{L2}};$$

$$\text{PF}_c = \frac{h_{\text{pf}}}{F'h_{\text{pf}} + U_{\text{tpa}}};\quad (\alpha\tau)_{1\text{eff}} = (\alpha_c - \eta_c)\tau_g\beta_c;$$

$$(\alpha\tau)_{2\text{eff}} = \alpha_p\tau_g^2(1-\beta_c);\ (\alpha\tau)_{\text{meff}} = \left[(\alpha\tau)_{2\text{eff}} + \text{PF}_1(\alpha\tau)_{1\text{eff}}\right];$$

$$(\alpha\tau)_{\text{ceff}} = \text{PF}_c\cdot\alpha_p\tau_g;\quad A_m = \text{WL}_m;\quad A_c = \text{WL}_c;$$

$$A_cF_{\text{Rc}} = \frac{\dot{m}_fc_f}{U_{\text{Lc}}}\left[1 - \exp\left(\frac{-F'U_{\text{Lc}}A_c}{\dot{m}_fc_f}\right)\right];$$

$$A_mF_{\text{Rm}} = \frac{\dot{m}_fc_f}{U_{\text{Lm}}}\left[1 - \exp\left(\frac{-F'U_{\text{Lm}}A_m}{\dot{m}_fc_f}\right)\right];$$

$$\left(\text{AF}_R(\alpha\tau)\right)_1 = \left[A_cF_{\text{Rc}}(\alpha\tau)_{\text{ceff}} + \text{PF}_2(\alpha\tau)_{\text{meff}}A_mF_{\text{Rm}}\left(1 - \frac{A_cF_{\text{Rc}}U_{\text{Lc}}}{\dot{m}_fc_f}\right)\right];$$

$$\left(\text{AF}_RU_L\right)_1 = \left[A_cF_{\text{Rc}}U_{\text{Lc}} + A_mF_{\text{Rm}}U_{\text{Lm}}\left(1 - \frac{A_cF_{\text{Rc}}U_{\text{Lc}}}{\dot{m}_fc_f}\right)\right];$$

$$K_K = \left(1 - \frac{\left(\text{AF}_RU_L\right)_1}{\dot{m}_fc_f}\right);\quad \left(\text{AF}_R(\alpha\tau)\right)_{m1} = \text{PF}_2(\alpha\tau)_{\text{meff}}A_mF_{\text{Rm}};$$

$$\left(\text{AF}_RU_L\right)_{m1} = A_mF_{\text{Rm}}U_{\text{Lm}};\ K_m = \left(1 - \frac{A_mF_{\text{Rm}}U_{\text{Lm}}}{\dot{m}_fc_f}\right);$$

$$(\alpha\tau)_{\text{eff},N} = \frac{\left(\text{AF}_R(\alpha\tau)\right)_1}{(A_c + A_m)}\left[\frac{1-(K_K)^N}{N(1-K_K)}\right];$$

$$U_{L,N} = \frac{\left(\text{AF}_RU_L\right)_1}{(A_c + A_m)}\left[\frac{1-(K_K)^N}{N(1-K_K)}\right]$$

Expressions for a_2 and $\bar{f}_2(t)$ used in Eq. (4) and expressions of different terms used in Eqs. (5)–(9) are as follows.

$$a_2 = \frac{1}{M_w C_w}\left[\begin{array}{l} \dot{m}_f C_f\left(1-K_k^N\right)+U_b A_b+\dfrac{h_{1\mathrm{wE}}\left(P-A_2\right)A_b}{2P}+ \\ \dfrac{h_{1\mathrm{wW}}\left(P-B_2\right)A_b}{2P} \end{array}\right];$$

$$\bar{f}_2(t) = \frac{1}{M_w C_w}\left[\begin{array}{l} \left(\dfrac{\alpha'_w}{2}+h_1\alpha'_b\right)A_b\left(\bar{I}_{\mathrm{SE}}(t)+\bar{I}_{\mathrm{SW}}(t)\right)+ \\ \dfrac{\left(1-K_k^N\right)}{\left(1-K_k\right)}\left(\mathrm{AF}_R(\alpha\tau)\right)_1\bar{I}_c(t)+ \\ \left(\dfrac{\left(1-K_k{}^N\right)}{\left(1-K_k\right)}\left(\mathrm{AF}_R U_L\right)_1+U_b A_b\right)\bar{T}_a+ \\ \left(\dfrac{h_{1\mathbf{wE}}A_1+h_{1\mathrm{wW}}B_1}{P}\right)\dfrac{A_b}{2} \end{array}\right]$$

$$A_1 = R_1 U_1 A_{gE} + R_2 h_{\mathrm{EW}} A_{\mathrm{gW}};$$

$$A_2 = h_{1\mathrm{WE}} U_2 \frac{A_b}{2} + h_{\mathrm{EW}} h_{1\mathrm{WW}} \frac{A_b}{2};$$

$$P = \left(U_1 U_2 - \frac{h_{\mathrm{EW}}^2}{A_{\mathrm{gE}}} h_{1\mathrm{WW}} \frac{A_b}{2}\right) A_{\mathrm{gW}};$$

$$U_1 = \frac{h_{1\mathrm{wE}}\dfrac{A_b}{2} + h_{\mathrm{EW}} A_{\mathrm{gE}} + U_{c,\mathrm{gaE}} A_{\mathrm{gE}}}{A_{\mathrm{gW}}};$$

$$U_2 = \frac{h_{1\mathrm{wW}}\dfrac{A_b}{2} + h_{\mathrm{EW}} A_{\mathrm{gW}} + U_{c,\mathrm{gaW}} A_{\mathrm{gW}}}{A_{\mathrm{gE}}};$$

$$B_1 = \frac{\left(R_2 P + A_1 h_{\mathrm{EW}}\right) A_{\mathrm{gW}}}{U_2 A_{\mathrm{gE}}};$$

$$B_2 = \frac{\mathrm{Ph}_{1\mathrm{wW}}\dfrac{A_b}{2} + h_{\mathrm{EW}} A_{\mathrm{gW}} A_2}{U_2 A_{\mathrm{gE}}};$$

$$R_1 = \alpha'_g I_{\mathrm{SE}}(t) + U_{c,\mathrm{gaE}} T_a;$$

$$R_2 = \alpha'_g I_{\mathrm{SW}}(t) + U_{c,\mathrm{gaW}} T_a$$

$$h_{\mathrm{EW}} = 0.034 \times 5.67 \times 10^{-8}\left[\left(T_{\mathrm{giE}}+273\right)^2+\left(T_{\mathrm{giW}}+273\right)^2\right]\left[T_{\mathrm{giE}}+T_{\mathrm{giW}}+546\right]$$

$$U_{c,\mathrm{gaE}} = \frac{\dfrac{K_g}{l_g}h_{1\mathrm{gE}}}{\dfrac{K_g}{l_g}+h_{1\mathrm{gE}}};\quad U_{c,\mathrm{gaW}} = \frac{\dfrac{K_g}{l_g}h_{1\mathrm{gW}}}{\dfrac{K_g}{l_g}+h_{1\mathrm{gW}}};$$

$$h_{1\mathrm{gE}} = 5.7 + 3.8\,V;\quad h_{1\mathrm{gW}} = 5.7 + 3.8\,V$$

$$h_{1\mathrm{wE}} = h_{\mathrm{rwgE}} + h_{\mathrm{cwgE}} + h_{\mathrm{ewgE}};$$

$$h_{1\mathrm{wW}} = h_{\mathrm{rwgW}} + h_{\mathrm{cwgW}} + h_{\mathrm{ewgW}};$$

$$h_{\mathrm{ewgE}} = 16.273 \times 10^{-3} h_{c,\mathrm{wgE}}\left[\frac{P_w - P_{\mathrm{giE}}}{T_w - T_{\mathrm{giE}}}\right];$$

$$h_{\mathrm{cwgE}} = 0.884\left[\left(T_w - T_{\mathrm{giE}}\right)+\frac{\left(P_w - P_{\mathrm{giE}}\right)\left(T_w+273\right)}{268.9\times10^3 - P_w}\right]^{\frac{1}{3}};$$

$$h_{\mathrm{ewgW}} = 16.273 \times 10^{-3} h_{c,\mathrm{wgW}}\left[\frac{P_w - P_{\mathrm{giW}}}{T_w - T_{\mathrm{giW}}}\right];$$

$$h_{\mathrm{cwgW}} = 0.884\left[\left(T_w - T_{\mathrm{giW}}\right)+\frac{\left(P_w - P_{\mathrm{giW}}\right)\left(T_w+273\right)}{268.9\times10^3 - P_w}\right]^{\frac{1}{3}};$$

$$P_w = \exp\left[25.317 - \frac{5{,}144}{T_w+273}\right]$$

$$P_{\mathrm{giE}} = \exp\left[25.317 - \frac{5{,}144}{T_{\mathrm{giE}}+273}\right];$$

$$P_{\mathrm{giW}} = \exp\left[25.317 - \frac{5{,}144}{T_{\mathrm{giW}}+273}\right];$$

$$h_{\mathrm{rwgE}} = \left(0.82\times5.67\times10^{-8}\right)\left[\left(T_w+273\right)^2+\left(T_{\mathrm{giE}}+273\right)^2\right]\left[T_w+T_{\mathrm{giE}}+546\right];$$

$$h_{\mathrm{rwgW}} = \left(0.82\times5.67\times10^{-8}\right)\left[\left(T_w+273\right)^2+\left(T_{\mathrm{giW}}+273\right)^2\right]\left[T_w+T_{\mathrm{giW}}+546\right];$$